A contact model to simulate human-artifact interaction based on force optimization: implementation and application to the analysis of a training machine

Daniel Krüger* and Sandro Wartzack

Friedrich-Alexander Universität Erlangen-Nürnberg (FAU), Germany

ARTICLE HISTORY
Compiled November 6, 2017

ABSTRACT
Musculoskeletal multibody models are increasingly used to analyze and optimize physical interactions between humans and technical artifacts. Since interaction is conveyed by contact between the human body and the artifact, a computationally robust modeling approach for frictional contact forces is a crucial aspect. In this contribution, we propose a parametric contact model and formulate an associated force optimization problem to simultaneously estimate unknown muscle and contact forces in an inverse dynamic manner from a prescribed motion trajectory. Unlike existing work, we consider both the static and the kinetic regime of Coulomb's friction law. The approach is applied to the analysis of a leg extension training machine with the objective to reduce the stress on the tibiofemoral joint. The uncertainty of the simulation results due to a tunable parameter of the contact model is of particular interest.

KEYWORDS
musculoskeletal simulation; contact modeling; optimization; device design

1. Introduction

Musculoskeletal simulations based on multibody dynamics are increasingly used to analyze and optimize interactions between human beings and technical artifacts like vehicles (Rasmussen et al. 2012), manufacturing systems (Kim and Lee 2009) and orthotic devices (van den Bogert 2003). The human musculoskeletal system is thereby regarded as a set of articulated rigid bodies driven by musculotendon actuators. For a technical artifact, a multibody representation can be derived from virtual CAD prototypes (Krüger and Wartzack 2014), which is merged with the musculoskeletal model to obtain a combined human-artifact system (Figure 1). In order to analyze the system's dynamic behavior, the methods of forward and inverse dynamics are applicable. In either case a crucial aspect is the consideration of contact forces, which convey physical interactions between the human body and the artifact. In a forward dynamics simulation, a time-stepping scheme is used to predict the kinematics of the system in dependence upon acting forces (Piazza 2006; Thelen et al. 2003). Contacts are typically modeled in terms of penalty forces that counteract a mutual penetration of the respective bodies. The penalty approach is appealing because it can be implemented in a simple way by means of springs and dampers whose parameters (e.g. contact stiffness) have a direct physical meaning (Anderson and Pandy 1999). Forward dynamics is a powerful simulation technique because it mimics the natural process of how human motion is generated. Especially for systems with contacts, however, very small integration time steps are required to yield robust results, which makes the method computationally quite demanding. In contrast, the inverse dynamics method relies on

* Corresponding author. Engineering Design; Department of Mechanical Engineering; Friedrich-Alexander Universität Erlangen-Nürnberg (FAU); Martensstrasse 9; 91058 Erlangen; Germany; daniel.krueger@fau.de; Tel. +49 9131 8523217; Fax. +49 913185 23223

linear equilibrium conditions to compute actuating forces that are physically consistent with a fixed (usually recorded) kinematic trajectory of the system. Its computational robustness does not depend on the discretization of the trajectory since it operates on individual time frames. Therefore the inverse dynamics method is particularly attractive for artifact design, where the principal value of a computer simulation is seen in the fast and reliable delivery of information rather than in revealing new scientific findings (Cecil and Kanchanapiboon 2007). Regarding contact modeling it must be noted that the input kinematics of an inverse dynamics simulation are usually subjected to measurement errors (Riemer et al. 2008) and thus do not provide physically consistent information on the mutual penetration (deformation, resp.) of contacting bodies, which impedes a direct evaluation of penalty force based contact models. An alternative approach for better complying with the idea of inverse dynamics, is to regard contact forces - like muscle forces - as actuating forces that are activated to keep the system on a predefined kinematic trajectory. This, however, can lead to an indeterminate synergy between muscles and contacts, which becomes evident in the example of a person who has put her hand on a car's gear lever: it is not clear what proportion of the arm's weight is carried by muscles and by contacts, respectively. Indeed this problem is very similar to the dynamic indeterminacy among (internal) muscle forces (Zajac 1993), which is often tackled using mathematical optimization techniques. Out of the many physically acceptable combinations of muscles forces, one is obtained that optimizes a certain performance criterion (Yamaguchi et al. 1995; Damsgaard et al. 2006). This idea can be extended to include also unknown contact (external) forces. Kerr and Roth (1986) solved a force optimization problem to determine the joint torques of a robotic manipulator grasping an object in the presence of contacts. Later, Robert et al. (2013) applied a similar procedure to a fullbody human model performing sit-to-stand movements. However, their model was torque driven and did not contain muscles. Recently, Fluit et al. (2014) predicted ground reaction and muscle forces for walking, descending stairs and squatting but it remains unclear if friction effects were considered in the contact model.

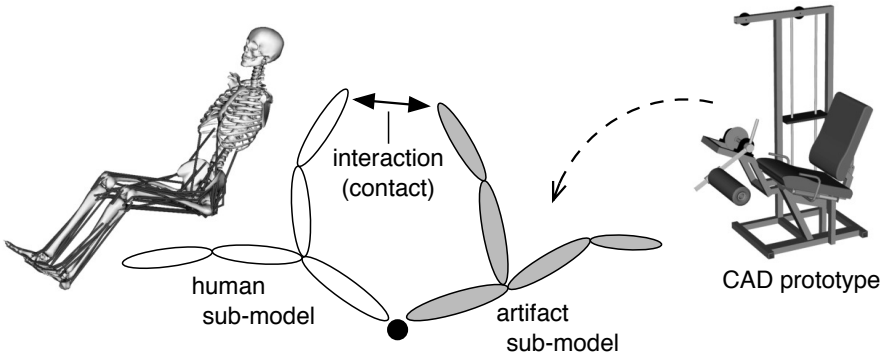

Figure 1. Topology of a combined human-artifact multibody system: physical interactions between the two sub-models entail dynamic loops that are closed by contact forces. The multibody representation of the artifact is derived from a virtual CAD prototype.

In this contribution we propose a parametric contact model and formulate an associated force optimization problem that allows the simultaneous estimation of internal muscle forces and contact forces in an inverse dynamic manner from a prescribed motion trajectory. Unlike existing work, we consider both the static and the kinetic friction regime and give a detailed description on how Coulomb's law is integrated into the force optimization problem. In order to illustrate the practical relevance we apply our approach to the analysis of a leg extension training machine. The objective is to reveal design adaptations that reduce the stress on the tibiofemoral joint during the execution of the exercise. The uncertainty of the simulation results due to a tunable parameter of the contact model is of particular interest.

2. General Methodology

2.1. *Parametric contact model*

Contact forces are surface forces that arise between two contacting bodies. If the bodies are assumed to be perfectly rigid they touch each other at discrete points. Depending on the shape of the bodies quite complex geometrical calculations are necessary to determine the exact location of these points at the surfaces (Jimnez et al. 2001). For the sake of clearness and without limiting the generality of our contact model, we consider the geometrical simple case of a point-on-plane contact (Figure 2). The contact area of the first body A is represented by a single point defined at a fixed location $\boldsymbol{p}$ with respect to the body's local reference frame. The surface of the second body B is approximated by an infinitely large plane. Contact is actually engaged if $\boldsymbol{p}$ lies within this plane. Nevertheless we allow that contact forces can be exchanged between the two bodies even for point to plane distances $d > 0$. Thus in general the contact force with respect to the plane body B acts at the orthogonal projection $\boldsymbol{p}^*$ and the force with respect to body A acts at $\boldsymbol{p}$ pointing in the opposite direction. Like all surface forces a contact force can be decomposed into three orthogonal components. In the following we refer to the force components acting on the plane body B for which we introduce the following parametric model:

$$\begin{aligned} \boldsymbol{F}_n &= -\lambda_n * \boldsymbol{n} * w(d) \\ \boldsymbol{F}_{s1} &= \lambda_{s1} * \boldsymbol{e}_1 * w(d) \\ \boldsymbol{F}_{s2} &= \lambda_{s2} * \boldsymbol{e}_2 * w(d) \end{aligned} \tag{1}$$

The normal component $\boldsymbol{F}_n$ is directed in the negative direction of the plane's normal vector $\boldsymbol{n}$. The two shear components $\boldsymbol{F}_{s1}$ and $\boldsymbol{F}_{s2}$ arise due to friction and inhibit a relative motion along the contact surface. They act along two orthonormal directions $\boldsymbol{e}_1$ and $\boldsymbol{e}_2$ that lie within the plane. The multipliers $\lambda_n, \lambda_{s1}, \lambda_{s2}$ control the magnitude of each force component. In addition, we introduce a weighting function $w(d)$ that scales the entire contact forces system dependent on the point-to-plane distance d. It is important to notice that $w(d)$ - unlike a spring - does not enforce a strict relationship between kinematics and force. The effective magnitude of the contact force is determined by setting the multipliers $\boldsymbol{\lambda}$ in the superordinate force optimization problem. Thus the contact model behaves similar like a muscle actuator which is gradually weakened as the two bodies move away from each other.

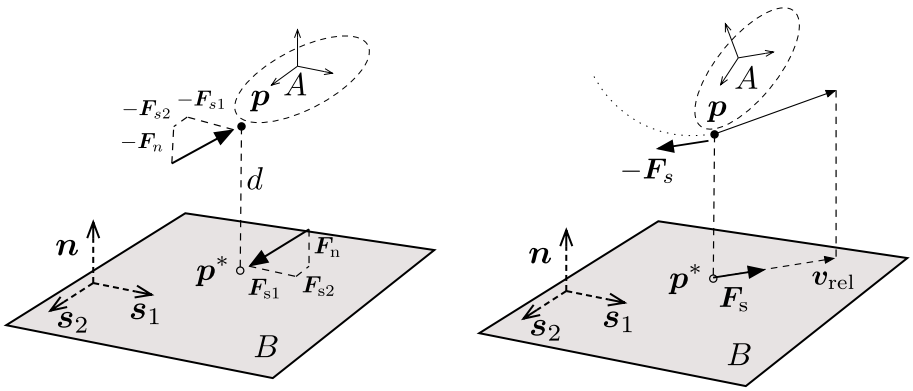

Figure 2. Point-on-plane contact: contact force components (left) and relative velocity in the contact area (right). Note that $\boldsymbol{v}_{\mathrm{rel}}$ is the relative velocity of the point with respect to the plane, expressed in the reference frame of the plane.

The dependency between the normal and the shear components are modeled according to Coulomb's law for dry friction (Popov 2010), which distinguishes between a static (sticking) and a kinetic (sliding) regime. Depending on the regime, different conditions have to be posed on the shear components. Let $\boldsymbol{v}_{\mathrm{rel}}$ be the relative velocity of point $\boldsymbol{p}$ with respect to the plane body B projected into the plane (Figure 2, right). The contact is in the static friction regime if $|\boldsymbol{v}_{\mathrm{rel}}| = 0$. In this case the shear components are free to take arbitrary values as long as they

stay within the friction cone. This can be formulated as an inequality condition on the contact multipliers:

$$\sqrt{\lambda_{s1}^2 + \lambda_{s2}^2} \leq \lambda_n \cdot \mu_s \tag{2}$$

In (2) μ_s is the static friction coefficient, which depends on the materials and the surface qualities of the contacting bodies.

If there is considerable relative motion in the contact area ($\boldsymbol{v}_{\text{rel}} \geq 0$), the contact is in the kinetic friction regime. In this case the shear components are clearly determined by the normal component, the kinetic friction coefficient μ_k and the relative velocity so that the two multipliers λ_{s1} and λ_{s2} have no effect on the contact force system:

$$\boldsymbol{F}_s = \frac{\boldsymbol{v}_{rel}}{|\boldsymbol{v}_{rel}|} \cdot \boldsymbol{F}_n \cdot \mu_k \tag{3}$$

As the total shear force $\boldsymbol{F}_s$ (3) inhibits the relative motion between the point and the plane it must point into the direction of $\boldsymbol{v}_{\text{rel}}$.

2.2. *Force optimization problem with frictional contacts*

In order to obtain the contact forces and unknown actuator forces (e.g. muscles) from a given motion trajectory, the parametric contact model is embedded into a general force optimization problem. We therefore consider a schematic multibody system (see Figure 3), whose equations of motion take the general form:

$$\mathbf{M}(\boldsymbol{q})\ddot{\boldsymbol{q}} - \boldsymbol{Q}(\boldsymbol{q}, \dot{\boldsymbol{q}}) = \boldsymbol{F}_{\text{p}}(\mathbf{t}, \boldsymbol{q}, \dot{\boldsymbol{q}}) + \boldsymbol{F}_{\mathbf{c}}(\boldsymbol{q}, \dot{\boldsymbol{q}}, \boldsymbol{\alpha}, \boldsymbol{\lambda}) \tag{4}$$

All quantities are expressed in the space of the generalized coordinates $\boldsymbol{q}$, which parametrize the kinematic configuration of the system. The mass matrix $\mathbf{M}$ captures the inertia properties of all rigid bodies. $\boldsymbol{Q}$ is a vector containing the velocity dependent gyroscopic and Coriolis forces. Forces that are externally applied to the multibody system are assumed to be either prescribed or controllable. The vector of prescribed forces $\boldsymbol{F}_p$ subsumes for example gravity, springs, dampers and the passive force components of muscles. Those are uniquely defined by either time t or the kinematic state $\boldsymbol{q}, \dot{\boldsymbol{q}}$ of the system. On the contrary, controllable forces $\boldsymbol{F}_c$ depend on additional parameters that are generally unknown in the inverse dynamic setting. At this point we focus on Hill-type musculotendon actuators controlled by an activity value α and contact forces (dependent on the multipliers $\boldsymbol{\lambda}$) according to the model described above. For the inverse dynamic analysis of the multibody system we presume that its kinematic trajectory is known and documented as a time series of generalized coordinates $\hat{\boldsymbol{q}}(t)$. An approximation of this position trajectory by a twice differentiable spline function delivers the velocities $\hat{\dot{\boldsymbol{q}}}(t)$ and the accelerations $\hat{\ddot{\boldsymbol{q}}}(t)$. At every instance in time the unknown muscle activities $\boldsymbol{\alpha}(t)$ and contact multipliers $\boldsymbol{\lambda}(t)$ are obtained as a solution of the following constrained optimization problem:

$$\begin{aligned}
&\underset{\boldsymbol{\alpha},\boldsymbol{\lambda}}{\text{minimize}} && f(\boldsymbol{\alpha}, \boldsymbol{\lambda}), && \boldsymbol{\alpha} \in \mathbb{R}^m, \boldsymbol{\lambda} \in \mathbb{R}^c && \text{(5a)}\\
&\text{subject to} && \boldsymbol{\alpha}_{\min} \leq \boldsymbol{\alpha} \leq \boldsymbol{\alpha}_{\max} && && \text{(5b)}\\
& && \boldsymbol{\lambda}_{\min} \leq \boldsymbol{\lambda} \leq \boldsymbol{\lambda}_{\max} && && \text{(5c)}\\
& && h_i(\boldsymbol{\alpha}, \boldsymbol{\lambda}) = 0, && i = 1, \ldots, n && \text{(5d)}\\
& && g_i(\boldsymbol{\lambda}) \geq 0, && i = 1, \ldots, k && \text{(5e)}
\end{aligned}$$

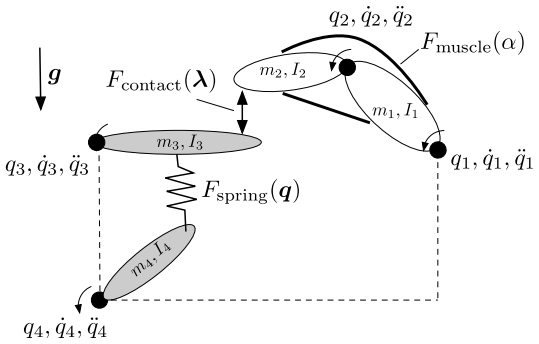

Figure 3. Schematic multibody system with prescribed and controllable forces.

2.2.1. Objective function

In a force optimization problem, the objective function (5a) reflects a hypothesis concerning the load distribution between redundant forces acting on the multibody system. In this contribution, the squared sum of all muscle activities and contact multipliers is minimized:

$$f(\boldsymbol{\alpha}, \boldsymbol{\lambda}) = \boldsymbol{\alpha}^\top \boldsymbol{\alpha} + \frac{1}{w_0} \cdot \boldsymbol{\lambda}^\top \boldsymbol{\lambda} \tag{6}$$

The activity α_i of a muscle is defined as the actual active fiber force normalized by the maximum force the fibers can generate at their current length and contraction velocity:

$$\alpha_i = \frac{F_i}{F_{i,max}(q, \dot{q})} \tag{7}$$

Therefore the first term in our objective function (6) fosters the recruitment of stronger muscles to relieve the weaker. According to Crowninshield and Brand (1981) this equals a minimization of fatigue, which is regarded as one of the governing principles of muscle coordination. A review of this and other optimization criteria to determine muscle forces is found by van Bolhuis and Gielen (1999). The second term in the objective function minimizes the squared sum of contact multipliers. Although this may be loosely related to Gauss' principle of least constraints (Redon et al. 2002), we use this formulation mainly because it allows us to gradually deactivate contacts that are geometrically not engaged: In the previous section we defined the magnitude of a contact force component as the product of a multiplier λ and a weighting function $w(d(\hat{\boldsymbol{q}}))$ dependent on the spatial distance between the contacting geometries. Similar to what is proposed by Fluit et al. (2014), we state this weighting function as:

$$w(d) = \frac{1}{2} \cdot \left[1 + \tanh\left(-\pi \cdot \frac{2(d - d_{\text{tol}}) - d_{\text{trans}}}{d_{\text{trans}}} \right) \right] \tag{8}$$

As the contacting geometries move away from each other, the weight on the contact force system decreases from an initial value of 1 down to 0 (see Figure 4). Thus, in the sense of the objective function (6), achieving a certain magnitude of contact force becomes more and more expensive since the corresponding multipliers $\boldsymbol{\lambda}$ have to be drastically increased in order to compensate the decline of $w(d)$. As a consequence, the contact is completely deactivated as soon as $w(d) = 0$.

The second term of the objective function (6) is reciprocally weighted by an additional factor w_0, which influences the global load distribution between muscle forces and contact forces. This shall be illustrated by the intuitive example depicted in Figure5. A block is resting on an inclined surface and can be pulled by an unknown muscle force $\boldsymbol{F}_m$. Since there is no motion, the sum of the friction force $\boldsymbol{F}_s$ and the muscle force $\boldsymbol{F}_m$ must balance out the downhill component $\boldsymbol{F}_{dg}$ of the gravity (see *dynamic equilibrium constraints* (11)). The load distribution is indeterminate.

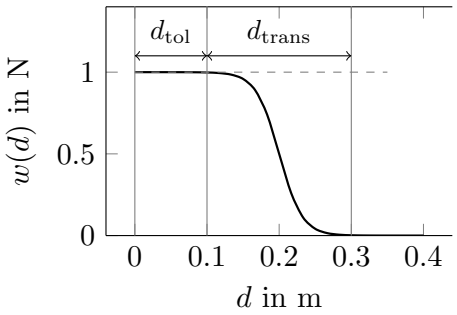

Figure 4. Weighting function assigned to a contact force system. With increasing distance between the contacting geometries the contact becomes gradually *weaker* until it is completely deactivated.

For very huge values of w_0, using the friction force is *inexpensive* so the muscle will not be recruited at all. As w_0 is decreased, the load is shifted more and more to the muscle until the friction force vanishes. It is intuitively understandable that the load distribution can be deliberately controlled by a human being without violating the laws of physics. Thus there is no preferable or physically reasonable value of w_0. In fact, this parameter introduces an uncertainty to the simulation results, which has to be considered.

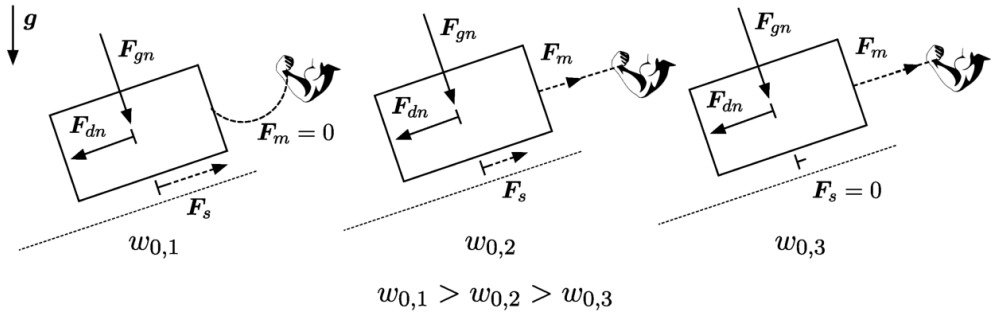

Figure 5. Block example demonstrating the effect of the parameter w_0: for huge values the bigger share of the load is carried by the contact forces. The load is shifted more to the muscles as w_0 is decreased.

2.2.2. Variable bounds

The optimization problem is further subject to bound constraints on the muscle activities (5b) and contact multipliers (5c). The bounds on the muscle activities stem naturally from the definition (7) to:

$$\boldsymbol{\alpha}_{\min} = 0.0,\ \boldsymbol{\alpha}_{\max} = 1.0 \tag{9}$$

Of the three multipliers that control a contact force system only the normal force multiplier λ_n needs to be directly constrained. The unilateral bound

$$\lambda_{\text{n,min}} = 0.0,\ \lambda_{\text{n,max}} = +\infty \tag{10}$$

avoids forces that would pull the two contacting bodies towards each other.

2.2.3. Dynamic equilibrium constraints

The equality constraints $h_i(\boldsymbol{\alpha}, \boldsymbol{\lambda})$ enforce the consistency between the muscle activities, the contact multipliers and the equations of motion (4). The dynamic equilibrium is formulated at the acceleration level defining that the generalized accelerations of the system due to $\boldsymbol{\alpha}, \boldsymbol{\lambda}$ exactly

match the known accelerations $\hat{\ddot{\boldsymbol{q}}}$ that are prescribed by the kinematic trajectory. Thus the number of equality constraints n equals the number of generalized coordinates in the multibody system. In a vectorial representation the constraint equations (5d) take the following form:

$$\boldsymbol{h}(\boldsymbol{\alpha}, \boldsymbol{\lambda}) = \ddot{\boldsymbol{q}}_0 + \mathbf{A} \cdot [\boldsymbol{\alpha}, \boldsymbol{\lambda}]^\top - \hat{\ddot{\boldsymbol{q}}} = \mathbf{0} \tag{11}$$

Here $\ddot{\boldsymbol{q}}_0$ are the generalized accelerations caused only by the prescribed forces $\boldsymbol{F}_\mathrm{p}$. It can be computed by a forward dynamic evaluation of the equations of motion with all muscle activities and contact multipliers set to zero:

$$\ddot{\boldsymbol{q}}_0 = \mathbf{M}(\hat{\boldsymbol{q}})^{-1}\big[\boldsymbol{F}_\mathrm{p}(\mathbf{t}, \hat{\boldsymbol{q}}, \hat{\dot{\boldsymbol{q}}}) + \boldsymbol{Q}(\hat{\boldsymbol{q}}, \hat{\dot{\boldsymbol{q}}}) + \boldsymbol{F}_\mathrm{c}(\hat{\boldsymbol{q}}, \hat{\dot{\boldsymbol{q}}}, \boldsymbol{\alpha} = \mathbf{0}, \boldsymbol{\lambda} = \mathbf{0})\big] \tag{12}$$

The matrix $\mathbf{A}$ contains the sensitivities of the actual generalized accelerations of the system with respect to changes in the muscle activities and contact multipliers. It has the following structure:

$$\mathbf{A} = \begin{bmatrix} \frac{\partial \ddot{q}_1}{\partial \alpha_1} & \cdots & \frac{\partial \ddot{q}_1}{\partial \alpha_m} & \frac{\partial \ddot{q}_1}{\partial \lambda_1} & \cdots & \frac{\partial \ddot{q}_1}{\partial \lambda_c} \\ \vdots & \ddots & \vdots & \vdots & \ddots & \vdots \\ \frac{\partial \ddot{q}_n}{\partial \alpha_1} & \cdots & \frac{\partial \ddot{q}_n}{\partial \alpha_m} & \frac{\partial \ddot{q}_n}{\partial \lambda_1} & \cdots & \frac{\partial \ddot{q}_n}{\partial \lambda_c} \end{bmatrix} \tag{13}$$

For a fixed kinematic configuration the relationship between the actuating forces and the resulting generalized accelerations of the multibody system is linear. Thus the partial derivatives in (13) can be exactly computed by finite differences applying unit-perturbations to the elements of $\boldsymbol{\alpha}$ and $\boldsymbol{\lambda}$ and evaluate the resulting accelerations $\ddot{\boldsymbol{q}}(\boldsymbol{\alpha}, \boldsymbol{\lambda})$ in analogy to (12):

$$\begin{aligned} \frac{\partial \ddot{\boldsymbol{q}}}{\partial \alpha_i} &= \ddot{\boldsymbol{q}}|_{\boldsymbol{\lambda}=\mathbf{0}, \alpha_i=1, \alpha_{j\neq i}=0} - \ddot{\boldsymbol{q}}_0 \\ \frac{\partial \ddot{\boldsymbol{q}}}{\partial \lambda_i} &= \ddot{\boldsymbol{q}}|_{\boldsymbol{\alpha}=\mathbf{0}, \lambda_i=1, \lambda_{j\neq i}=0} - \ddot{\boldsymbol{q}}_0 \end{aligned} \tag{14}$$

2.2.4. Friction cone constraints

Due to the consideration of friction, additional constraints $\boldsymbol{g}_i(\boldsymbol{\lambda})$ have to be defined on the contact multipliers that couple the shear forces to the normal forces according to Coulomb's law. A direct transcription of the friction cone condition (2) results in one *nonlinear* inequality constraint equation for each contact in the multibody system.

$$g_i = \lambda_n^2 \cdot \mu_s^2 - \lambda_{s1}^2 - \lambda_{s2}^2 \geq 0 \tag{15}$$

Since all the other constraints are linear, we prefer a linear approximation of (15) to facilitate the numerical solution of the optimization problem. This is achieved by circumscribing the friction cone with a pyramid (see Figure 6), which results in four linear inequality constraints per contact:

$$\begin{aligned} g_i &= \lambda_{s1} + \lambda_n \cdot \mu_s &&\geq 0 \\ g_{i+1} &= -\lambda_{s1} + \lambda_n \cdot \mu_s &&\geq 0 \\ g_{i+2} &= \lambda_{s2} + \lambda_n \cdot \mu_s &&\geq 0 \\ g_{i+3} &= -\lambda_{s2} + \lambda_n \cdot \mu_s &&\geq 0 \end{aligned} \tag{16}$$

Unlike the bound constraint on the normal multiplier (10), these friction cone constraints are only included in the optimization problem if the respective contact is in the static regime of Coulomb's law. For the point-in-plane contact this is the case if $|\boldsymbol{v}_\mathrm{rel}| \leq v_\mathrm{trans}$, where $\boldsymbol{v}_\mathrm{rel}$ is the relative in-plane velocity between the point and the plane which can be computed from

the kinematic trajectory and $v_{trans} > 0$ is a user definable transition velocity. Otherwise if the contact is in the kinetic regime, the friction forces depend only on the normal force components and are computed according to (3).

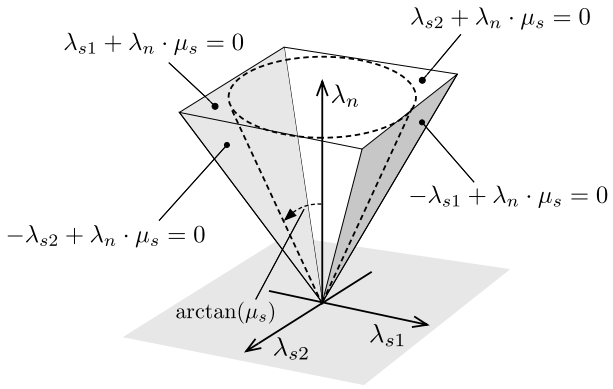

Figure 6. In the static regime of Coulomb's law the shear components of a contact force must reside within the friction cone, which is linearly approximated by a pyramid here.

2.3. *Implementation*

We implemented our approach as a plug-in for OpenSim (Delp et al. 2007), a software platform to create and analyze detailed dynamic simulation models of human and animal musculoskeletal systems. Our plug-in adds a point-on-plane contact element to OpenSim's modeling library and provides an analysis algorithm that solves the force optimization problem by applying an interior point method (Wächter and Biegler 2006).

The source code and a binary distribution of the plug-in are freely available on `https://simtk.org/projects/statopt-contact`.

3. Application: Analysis of a leg extension training machine

3.1. *Objective*

The practical relevance of our approach is illustrated by the analysis of a leg extension training machine. Leg extensions are a resistance weight exercise aimed at strengthening the *m. quadriceps femoris*. The exercise is performed in a seated position whereby the knee is extended against a resistance force. In the typical design of the machine the resistance force is applied to the *tibia* via a padded lever which is driven by a pulley mechanism (Figure 7). The crucial part of this mechanism is a cam that transforms the training weight into a torque $\tau_{\text{res.}}$ acting on the lever axis. Effectively, the shape of this cam determines the relationship between the resistance force $\boldsymbol{F}_{\text{res.}}$ (applied to the *tibia*) and the knee flexion angle β_{knee}. We like to approach the question if the shape of the cam is a suitable design parameter to optimize the training conditions. Two aspects have to be considered: on the one hand, a high metabolic exhaustion of the muscle is desirable to promote its formation. On the other hand, leg extensions are deemed to put excessive stress on the articular cartilage and the cruciate ligaments. The latter is especially an issue when the exercise is performed in rehabilitation after an ACL restoration. We therefore decided to examine tibiofemoral joints loads and the mechanical muscle power generated by *m. quadriceps femoris* for two different cam designs by means of a combined human-artifact multibody simulation.

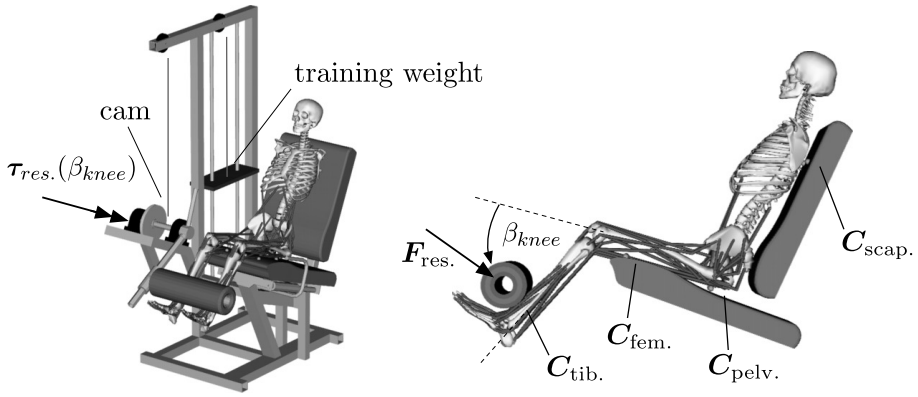

Figure 7. Simulation model of the training machine. Contacts between the human model and the artifact model are placed between tibia and bracket, femur and seat (2 points), pelvis and seat as well as between scapula and backrest.

3.2. *Simulation model and design of experiments*

For this case study a musculoskeletal human model of the lower extremity was used, which is based on the work of Delp et al. (1990). The model (Figure 7) represents a male subject of about 1.8 m body height and 75 kg weight. It has 23 degrees of freedom which are driven by 96 musculotendon actuators. The patellofemoral and tibiofemoral joints are modeled as planar joints with rotations and translations coupled to the knee flexion angle in order to simulate rolling and gliding (Yamaguchi and Zajac 1989). Even though this knee model does not contain any ligaments, DeMers et al. (2014) were able to show that it predicts realistic joint reaction forces for walking. All musculoskeletal parameters of the model were kept at their default values. The product model of the leg extension machine was composed using a parametric CAD environment (PTC Creo). The resistance torque $\tau_{\text{res.}}$ is prescribed dependent on the knee flexion angle β_{knee} whereby the exact relationship is computed within the CAD environment according to the shape of the cam. Contact between the human model and the training machine is modeled by 10 discrete point-on-plane contact elements as shown in Figure7. To construct a motion trajectory of the exercise, we employed an inverse kinematic technique prescribing a bell-shaped velocity profile so that the knee is extended from $\beta_{knee} = -95°$ to $\beta_{knee} = -5°$ within 5 seconds.

Two different cam designs were examined. Cam_1 is a is a circular disc leading to a constant training resistance throughout the extension of the knee. Cam_2 is formed elliptical. It produces a rising resistance profile that reaches its peak value when the knee approaches the extended position. The corresponding torque profiles are depicted in Figure8. In both cases the peak value was set to 50 N m, which is a relatively moderate training intensity.

The intuitive example in Figure 5 showed, that the global weight factor w_0 assigned to the contact term in the objective function (6) controls the indeterminate load distribution between muscle and contact forces. To understand this effect for the case of the leg extension machine we performed a sensitivity analysis of contact forces and joint torques with respect to w_0 before we actually computed the metrics of interest (tibiofemoral joint loads and muscle power) for the two cam designs. The sensitivity was determined by running every simulation three times: a first trial with a low weight factor of $w_0 = 1.0$, a second trial with the factor increased to $w_0 = 500.0$ and a third trial with a huge value of $w_0 = 1000.0$.

3.3. *Results*

3.3.1. Load distribution between muscle and contact forces

The sensitivity analysis with regard to w_0 revealed a dynamic indeterminacy within the hip flexion degree of freedom of the simulation model. This can be seen in the divergent hip flexion

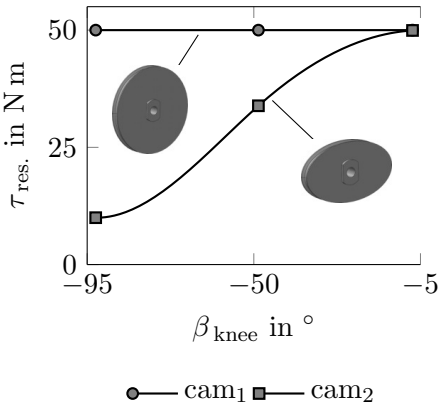

Figure 8. Resulting resistance torque profiles for two different cam designs

torque τ_{hip} due to different values for w_0 (Figure 9). The muscles that flex the hip joint compete with the contacts $\boldsymbol{C}_{\text{fem.}}$ located at the distal end of the femur. A low w_0 makes the utilization of these contacts more expensive for the optimizer. Thus a greater share of the load is carried by the muscles. This reflects a situation where the exercise is done *out of the hip* avoiding contact with the front edge of the seat. If the weight factor is increased to $w_0 = 500.0$ the load is shifted more towards the contacts. A further increase to $w_0 = 1000.0$ does not lead to much different results, which points to a converging behavior of the simulation.

For the knee extension torque this effect was not observed. However, since the hip flexor *m. rectus femoris* also contributes to the extension of the knee, the setting of w_0 is expected to have an effect on the tibiofemoral joint loads as well.

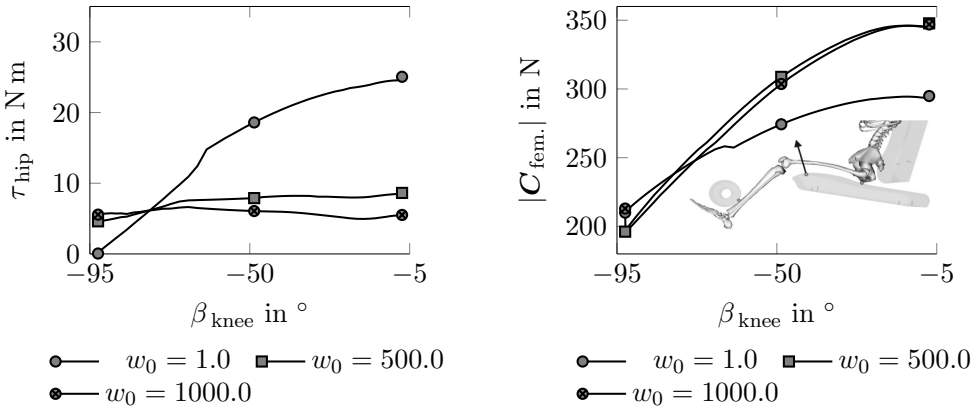

Figure 9. Dynamic indeterminacy within the hip flexion degree of freedom: the contacts at the distal femur compete with the muscles that flex the hip. The load distribution is influenced by the contact weight factor w_0.

3.3.2. Tibiofemoral joint loads

The tibiofemoral joint loads for cam$_1$ and cam$_2$ are shown in Figure 10. Qualitatively, these results agree well with experimental examinations published by Escamilla et al. (1998). It must, however, be taken into account that the exact resistance torque profile was not documented in that study. Each curve is the arithmetic mean of three simulation runs with varying contact weight factors ($w_0 = 1.0$, $w_0 = 500.0$ and $w_0 = 1000.0$) whereby the shaded areas indicate the uncertainty of the results. The uncertainty is generally greater when the training resistance is low (cam$_2$) but in general the impact of the factor w_0 is not substantial, as it does not question the main finding of this examination: the shape of the cam has a notable impact on the tibiofemoral joint loads during the exercise. With the elliptical cam$_2$ the maximum

posteroanterior shear force is reduced by about 150 N compared to the circular cam_1. In reality (not in the simulation model), shear forces at the knee are mainly absorbed by the cruciate ligaments, the articular capsule and also by the patellofemoral joint. At higher flexion angles the capsule is quite flaccid and thus provides little stability to the knee (Nordin and Frankel 2012). Consequently, it is regarded advantageous that cam_2 reduces the load during this critical initial phase of the extension motion. For the compression forces the relief due to cam_2 is even greater (Figure 10, right).

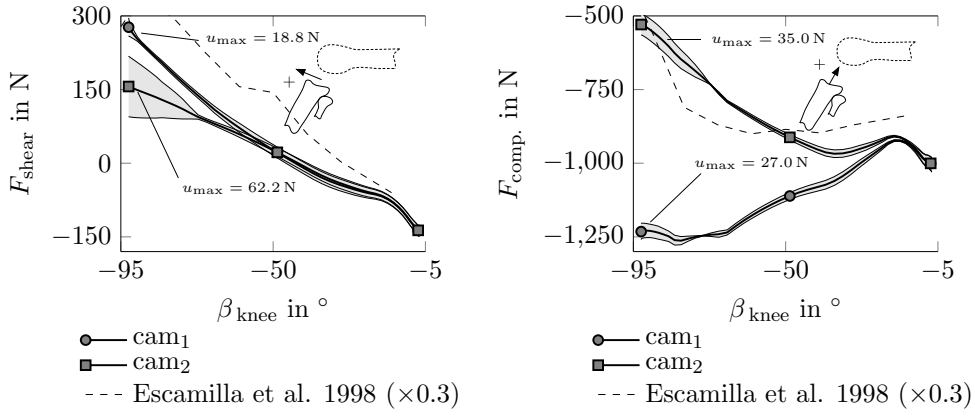

Figure 10. Tibiofemoral shear (left) and compression forces (right) expressed with respect to the tibia. The uncertainties, due to the setting of the contact weight factor (shaded areas), are drawn twice as high as in reality. The results show good qualitative agreement with joint loads calculated from EMG data published by Escamilla et al. (1998)

3.3.3. Muscle power

Reducing the training intensity at greater flexion angles by using cam_2 of course leads to a loss of metabolic turnover in *m. quadriceps femoris* compared to a constant resistance profile. In order to quantify this loss we did not apply a physiological model of muscle metabolics (Umberger et al. 2003) but computed the summed mechanical power produced by the four quadriceps heads during one extension of the leg. The result is depicted in Figure 11. The shaded area between the curves equals the loss of mechanical muscle work due to the different cam designs. We assume that this loss of 21.3 % is tolerable considering that the elliptic cam_2 in return reduces the stress on the tibiofemoral joint in the critical flexed position of the knee.

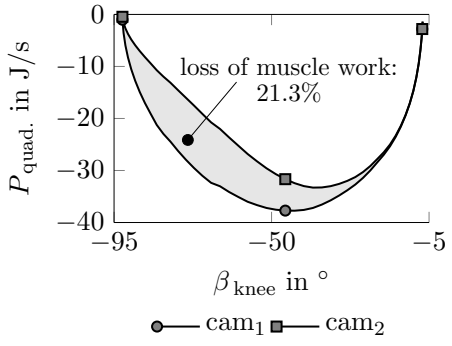

Figure 11. Total mechanical power generated by *m. quadriceps femoris*. The shaded area between the curves represents the loss of muscle work when using cam_2 instead of cam_1.

4. Discussion

In this contribution we described a force optimization procedure to solve indeterminate inverse dynamic problems including contacts with Coulomb friction, which arise particularly in analyses of human-artifact interactions. Unlike similar approaches, we also considered the kinetic regime of Coulomb's law by switching the structure of the optimization problem depending on the sliding velocity at the points of contact.

A general characteristic of force optimization approaches is that the results depend on the load distribution hypothesis represented by the objective function whenever the system is in a state of dynamic indeterminacy. This is the case if multiple unknown forces (e.g. contacts and muscles) act upon the same degree of freedom.

In the presented approach, the crucial parameter that influences the load distribution between contact forces and muscle forces is the weight factor w_0 assigned to the contact term of the objective function. The intuitive example of a block resting on an inclined surface but also the analysis of the leg extension machine showed that w_0 can be interpreted to reflect the human freedom of action under given physical constraints. It is important to notice that w_0 does not influence the physical validity of the results as the equations of motion (4) and Coulomb's law (2) are strictly enforced during the optimization. However, depending on the specific problem it may be possible to identify a preferable setting. In case of the leg extension machine for example, setting w_0 to huge values is expected to be more realistic than very low values because humans tend to relieve their muscles if possible. In general, however, we suggest to explicitly consider the uncertainty of the simulation results with regard to the setting of w_0. In practical terms this means that all simulations have to be run several times with varying w_0 in order to obtain an estimate for the result variation.

References

Anderson FC, Pandy MG. 1999. A dynamic Optimization Solution for Vertical Jumping in Three Dimensions. Comput Methods Biomech Biomed Eng. 2(3):201–231.

Cecil J, Kanchanapiboon A. 2007. Virtual engineering approaches in product and process design. Int J Adv Manuf Technol. 31(9-10):846–856.

Crowninshield R, Brand R. 1981. A physiologically based criterion of muscle force prediction in locomotion. J Biomech. 14:793–801.

Damsgaard M, Rasmussen J, Christensen ST, Surma E, de Zee M. 2006. Analysis of musculoskeletal systems in the AnyBody Modeling System. Simul Model Pract Th. 14:1100–1111.

Delp S, Anderson F, Arnold A, Loan P, Habib A, John C, Guendelman E, Thelen D. 2007. OpenSim: Open-Source Software to Create and Analyze Dynamic Simulations of Movement. IEE Trans Biomed Eng. 54:1940–1950.

Delp S, Loan J, Hoy M, Zajac F, Topp E, Rosen J. 1990. An interactive graphics-based model of the lower extremity to study orthopaedic surgical procedures. IEEE Trans Biomed Eng. 37:757–767.

DeMers MS, Pal S, Delp SL. 2014. Changes in tibiofemoral forces due to variations in muscle activity during walking. J Orthop Res. 32:769–776.

Escamilla RF, Fleisig GS, Zheng N, Barrentine SW, Wilk KE, Andrews JR. 1998. Biomechanics of the knee during closed kinetic chain and open kinetic chain exercises. Med Sci Sports Exerc. 30(4):556–569.

Fluit R, Andersen M, Kolk S, Verdonschot N, Koopman H. 2014. Prediction of ground reaction forces and moments during various activities of daily living. J Biomech. 47:2321–2329.

Jimnez P, Thomas F, Torras C. 2001. 3d collision detection: a survey. Comput Graph. 25:269–285.

Kerr J, Roth B. 1986. Analysis of Multifingered Hands. Int J Robot Res. 4:3–17.

Kim SH, Lee K. 2009. Development of discomfort evaluation method for car ingress motion. Int J Automot Technol. 10:619–627.

Krüger D, Wartzack S. 2014. Towards CAD integrated simulation of use under ergonomic aspects. In: Marjanovic D, Culley S, Lindemann U, McAloone T, Weber C, editors. Proceedings of the DESIGN 2014 13th International Design Conference; 2014 May 19-22; Dubrovnik(HR).

Nordin M, Frankel V. 2012. Basic biomechanics of the musculoskeletal system. Philadelphia: Lippincott Raven.

Piazza SJ. 2006. Muscle-driven forward dynamic simulations for the study of normal and pathological gait. J Neuroeng Rehabil. 3(5).
Popov VL. 2010. Contact mechanics and friction: physical principles and applications. New York: Springer.
Rasmussen J, Boocock M, Paul G. 2012. Advanced musculoskeletal simulation as an ergonomic design method. Work. 41:6107–6111.
Redon S, Kheddar A, Coquillart S. 2002. Gauss' least constraints principle and rigid body simulations. In: Hamel W, Maciejewski A, editors. Proceedings of ICRA'02 IEEE International Conference on Robotics and Automation; 2002 May 11-15; Washington, D.C.
Riemer R, Hsiao-Wecksler ET, Zhang X. 2008. Uncertainties in inverse dynamics solutions: A comprehensive analysis and an application to gait. Gait Posture. 27(4):578–588.
Robert T, Causse J, Monnier G. 2013. Estimation of external contact loads using an inverse dynamics and optimization approach: General method and application to sit-to-stand maneuvers. J Biomech. 46:2220–2227.
Thelen DG, Anderson FC, Delp SL. 2003. Generating dynamic simulations of movement using computed muscle control. J Biomech. 36(3):321–328.
Umberger BR, Gerritsen KG, Martin PE. 2003. A Model of Human Muscle Energy Expenditure. Comput Methods Biomech Biomed Eng. 6:99–111.
van Bolhuis BM, Gielen CC. 1999. A comparison of models explaining muscle activation patterns for isometric contractions. Biol Cybern. 81:249–261.
van den Bogert AJ. 2003. Exotendons for assistance of human locomotion. Biomed Eng Online. 2:1–8.
Wächter A, Biegler LT. 2006. On the implementation of an interior-point filter line-search algorithm for large-scale nonlinear programming. Math Prog. 106:25–57.
Yamaguchi G, Moran D, Si J. 1995. A computationally efficient method for solving the redundant problem in biomechanics. J Biomech. 28:999–1005.
Yamaguchi GT, Zajac FE. 1989. A planar model of the knee joint to characterize the knee extensor mechanism. J Biomech. 22:1–10.
Zajac FE. 1993. Muscle coordination of movement: A perspective. J Biomech. 26:109–124.

This is an Accepted Manuscript of an article published by Taylor & Francis in Computer Methods in Biomechanics and Biomedical Engineering on 30/10/2017, available online:
`http://www.tandfonline.com/10.1080/10255842.2017.1393804`